ACS Catalysis

Research Article

pubs.acs.org/acscatalysis

Mechanistic Insights into the Electrochemical Reduction of CO_2 to CO on Nanostructured Ag Surfaces

Jonathan Rosen,[†,§] Gregory S. Hutchings,[†,§] Qi Lu,[†] Sean Rivera,[†] Yang Zhou,[‡] Dionisios G. Vlachos,[†] and Feng Jiao*[,†]

[†]Center for Catalytic Science and Technology (CCST), Department of Chemical and Biomolecular Engineering, University of Delaware, 150 Academy Street, Newark, Delaware 19716, United States

[‡]Department of Physics and Astronomy, University of Delaware, Newark, Delaware 19716, United States

Supporting Information

ABSTRACT: Electroreduction of CO_2 in a highly selective and efficient manner is a crucial step toward CO_2 utilization. Nanostructured Ag catalysts have been found to be effective candidates for CO_2 to CO conversion. In this report, we combine experimental and computational efforts to explore the electrocatalytic reaction mechanism of CO_2 reduction on nanostructured Ag catalyst surfaces in an aqueous electrolyte. In contrast to bulk Ag catalysts, both nanoparticle and nanoporous Ag catalysts show enhanced ability to reduce the activation energy of the CO_2 to $COOH_{ads}$ intermediate step through the low-coordinated Ag surface atoms, resulting in a reaction mechanism involving a fast first electron and proton transfer followed by a slow second proton transfer as the rate-limiting step.

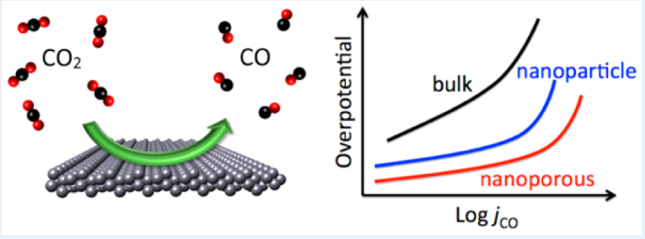

KEYWORDS: *carbon dioxide, electrocatalysis, silver, mechanism, nanostructure*

INTRODUCTION

Converting CO_2 to useful chemicals is an important research topic because the process can produce carbon-neutral fuels and reduce greenhouse gas emissions simultaneously.[1−6] Electrochemical CO_2 reduction using metallic catalysts has shown great promise.[7−12] Gold and silver are of particular interest, since both metals exhibit extremely good CO selectivity under moderate overpotentials in comparison to other metallic catalysts.[11,13−16] High CO_2 reduction selectivity is important for future commercialization of these technologies because expensive separation processes can be avoided, decreasing the overall cost of scale-up. In addition, lowering the overpotential or energy penalty is of great importance for decreasing the energy needed to drive the reaction. Prior existing literature has shown that the high CO selectivities of gold- and silver-based catalysts are due to the weak proton and CO binding strengths on their surfaces, which prevent CO from further deep reduction while suppressing hydrogen evolution.[11,17] Only at high overpotentials have trace amounts of other products such as formate been reported.[15]

Very recently, we have shown the enhanced CO_2 to CO reduction activity of a nanoporous Ag catalyst using an aqueous electrolyte in a near neutral pH environment.[14] The catalyst was synthesized through a dealloying process of a Ag−Al bimetallic alloy, which is straightforward and scalable for industrial processes. The resulting nanoporous structure creates an extremely large surface area for catalytic reactions and increased per surface site activity for CO_2 conversion, resulting in an exceptional activity that is over 3 orders of magnitude higher than that of the bulk counterpart, on a geometric basis, at significantly decreased overpotentials of <500 mV. Moreover, such a remarkable activity for CO_2 electroreduction has been achieved with a CO Faradaic efficiency of 92%. We hypothesize that the increase in per surface site activity is due to the increase in step site density, but currently the source of the improvement and overall mechanism are not well understood.

Here, we have performed a series of studies to reveal the fundamental reaction mechanism of CO_2 reduction to CO on highly nanostructured Ag catalyst surfaces. Not only have the key electrochemical steps of CO_2 to CO on nanostructured Ag-based catalysts been examined experimentally but also the proposed catalytic reaction mechanism has been assessed computationally. The systematic investigation shows the effects of parameters such as electrolyte concentration, coverage effects, applied potential, and partial pressure on activity. Our results suggest that the kinetic rate-limiting step in CO_2 electroreduction to CO on nanostructured Ag surfaces is likely the protonation of the adsorbed $COOH_{ads}$. A better understanding of the key rate-determining steps will help in the rational design of better electrocatalysts requiring much lower overpotential to overcome the kinetic limitations.

Received: October 6, 2014
Revised: June 4, 2015
Published: June 5, 2015

DOI: 10.1021/acscatal.5b00840
ACS Catal. 2015, 5, 4293−4299

EXPERIMENTAL SECTION

Computational Modeling. Relative free energy changes of adsorbed intermediates on model surfaces were computed using density functional theory (DFT) with the Vienna ab initio simulation package (VASP).[18−20] Full computational details, including a table of calculated thermodynamic properties, are provided in the Supporting Information. Briefly, Ag(100), Ag(111), Ag(110), and Ag(211) surfaces were modeled as 3 × 3 periodic surfaces with either four or three sublayers of atoms beneath the adsorption site and at least 15 Å of vacuum between layers. The top two layers and adsorbates were allowed to relax, and the electronic structure was calculated in a (5,5,1) *k*-point Monkhorst−Pack grid using the revised Perdew−Burke−Ernzerhof (RPBE) functional with spin polarization included and a plane-wave cutoff of 400 eV. For the final free energy diagrams, adsorbate configurations with the lowest energy were selected.

Synthesis of Ag Electrodes. Ag foil (Alfa Aesar, 99.998%) electrodes were first micropolished and sonicated in acetone, dilute HCl, and water, respectively, prior to electrochemical testing. To prepare the Ag nanoparticle electrodes, Ag nanoparticles (>100 nm, Sigma-Aldrich, 99.5% trace metals basis) were first suspended in a solution of 40 mg of catalyst, 2.4 mL of DI water, 2.4 mL of isopropyl alcohol, and 40 μL of Nafion solution (DuPont). Following high-power sonication, the solution was then uniformly coated onto a Sigracet 25BC gas diffusion layer to achieve a desired loading of 10 mg cm^{-2}. Nanoporous Ag electrodes were prepared through a previously described dealloying technique using Ag/Al slices with atomic ratio 20/80 in HCl solutions.[14] All materials were then attached to a piece of nickel wire using colloidal silver paint for use in electrochemical testing.

Structural Characterization. Powder X-ray diffraction (PXRD) measurements were performed using a PANalytical X'Pert X-ray diffractometer using Cu Kα radiation. Scanning electron microscopy (SEM) images were collected using a JEOL JSM-6330F instrument.

Electrochemical Testing. A Princeton Applied Research VersaSTAT 3 potentiostat was used for all electrochemical testing. CO_2 reduction experiments were performed in a gastight two-compartment electrochemical cell separated by a piece of anion exchange membrane (Fumasep, FAA-3-PK-130). The electrolyte was 0.5 M $NaHCO_3$ saturated with CO_2 with a pH of 7.2. The bicarbonate electrolyte was prepared by purging sodium carbonate (Fluka, ≥99.9999) with CO_2 gas overnight to convert to sodium bicarbonate. A platinum wire was used as the counter electrode and Ag/AgCl (3.0 M NaCl saturated with AgCl, BASi) as the reference electrode. The reference electrode potentials were converted to RHE using the formula $E(\text{RHE}) = E(\text{Ag/AgCl}) + 0.210\ \text{V} + 0.0591\ \text{V} \times \text{pH}$. Additionally, the potentials on an RHE scale were converted to overpotential with the formula $E(\eta) = E(\text{RHE}) + 0.11\ \text{V}$. It is important to note that the true reversible potential assumes a constant CO partial pressure. Under experimental conditions, this concentration is small and therefore this formula works as an accurate reference potential.

Prior to electrolysis the bicarbonate electrolyte was purged with CO_2 gas for at least 30 min, and the headspace was then purged for at least 10 min. The electrolyte in the cathodic compartment was stirred to help assist in diffusion of gas reactants and products. In the case of polycrystalline Ag, the electrolyte was further purified using a 2 h pre-electrolysis with a sacrificial nanoporous Ag electrode prior to testing, in order to minimize the effects of any impurities in the electrolyte. Gas phase product quantification was performed using a gas chromatograph (Shimadzu, GC-2014) equipped with PLOT MolSieve 5A and Q-bond PLOT columns. Helium (99.999%) was used as the carrier gas. Gas-phase products were collected every 30 min using a gastight syringe (Hamilton) to access catalyst selectivity and total partial current density. Liquid product analysis was done on a Bruker AVIII 600 MHz NMR spectrometer: a 500 μL electrolyte was sampled at the conclusion of the electrolysis and mixed with 100 μL of D_2O, and 1.67 ppm (m/m) of dimethyl sulfoxide (DMSO, Alfa Aesar, ≥99.9%) was added as the internal standard. The 1D ^{1}H spectrum was measured with water suppression using a presaturation method. Sample data for GC and NMR measurements are shown in Figure S1 in the Supporting Information.

To confirm that CO_2 was the source of CO on Ag catalysts, a series of control experiments were performed. Experiments where CO_2 was not purged into the bicarbonate electrolyte yielded no CO product. In addition, cyclic voltammetry experiments (Figure S2 in the Supporting Information) showed the activation of the CO_2 molecule in CO_2-purged electrolyte, while no such reduction peak was seen in N_2-purged solutions, ruling out the activation of bicarbonate by Ag electrodes. These experiments agree with our proposed mechanisms that dissolved CO_2 and not carbonate formed from purging is the source of the products.

The electrochemically active surface areas of Ag catalysts were measured using monolayer oxide oxidation. Measurements were conducted using a three-electrode electrochemical cell with a platinum-wire counter electrode and Ag/AgCl reference electrode. The electrolyte was 0.1 M KOH (Sigma-Aldrich) saturated with N_2. The Ag electrodes were first reduced for 10 min at −0.4 V vs RHE prior to oxidation at 1.15 V vs RHE. At 1.15 V vs RHE only a monolayer of oxide formed on the Ag surface. By measuring the charge passed during the oxidation process, relative surface area measurements could be made for all Ag catalysts. We also attempted to measure the electrochemical surface areas of Ag catalysts using the Pb underpotential deposition method, though the estimated surface was much smaller than the value estimated from the geometric configuration. This inconsistency could originate from the introduction of contaminants in that system and will be examined in future work.

Partial pressure dependence experiments were performed with CO_2 pressures varying from 0.1 to 1 atm. The partial pressure was controlled by purging the headspace of the cathodic compartment for 20 min before electrolysis with mixtures of CO_2 and N_2. The concentration-dependence experiments were performed by conducting electrolysis experiments in electrolytes with bicarbonate concentration from 0.1 to 1 M. $NaClO_4$ (Sigma-Aldrich, 99.99%) was then added to the electrolytes to maintain a constant salt concentration of 1 M. The pH value for each electrolyte as a function of salt and gas concentration can be found in Tables S1 and S2 in the Supporting Information, respectively. Each experiment was performed in the apparent Tafel slope region to ensure catalyst kinetics were the sole rate-determining step. CO partial current densities were calculated for all experiments by first measuring CO produced using gas chromotography and then converting to electrical charge passed. For the nanoparticle electrodes, partial pressure and concentration-dependence studies were performed at −0.450 V vs RHE. For the nanoporous silver catalysts, experiments were performed at −0.350 V vs RHE for the partial pressure study and −0.387 V vs RHE for the concentration-dependence study. For bulk Ag catalysts, partial pressure and concentration-dependence studies were performed at −0.8 V vs RHE.

RESULTS AND DISCUSSION

Recently, we have reported a nanoporous Ag catalyst with greatly enhanced performance over bulk Ag.[14] We hypothesized that the high density of stepped sites on the nanoporous surface led to increased stabilization of key intermediates and therefore improved CO_2 reduction activity. To further explore the feasibility of such a claim in the case of nanostructured Ag surfaces, we have calculated the free energy change of each proton−electron pair transfer in the mechanism of CO_2 to CO on various model Ag surfaces using DFT to see if the stepped surfaces could be the source of the improvement. A full description of the computational model, on the basis of the computational hydrogen electrode (CHE) model as implemented in previous studies on Cu and Au surfaces,[10,21,22] is provided in Table S3 in the Supporting Information.

Stepped Ag(211) and Ag(110) surfaces, which are much more prevalent in the nanostructured Ag catalysts in

DOI: 10.1021/acscatal.5b00840
ACS Catal. 2015, 5, 4293−4299

comparison to the bulk material, are considered alongside the flat Ag(111) and Ag(100) facets at an applied overpotential of −0.11 V vs RHE. It is clear from the calculations (Figure 1)

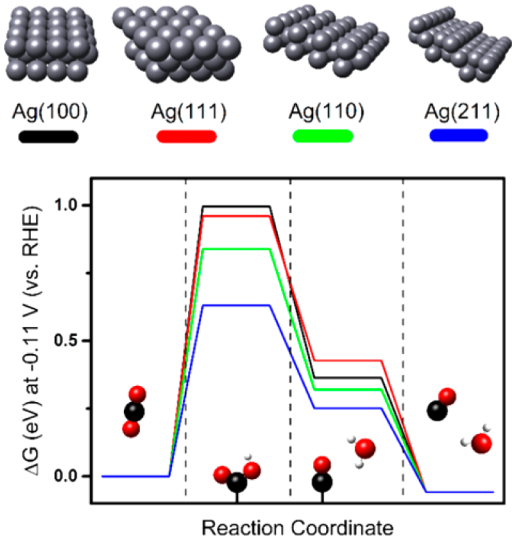

Figure 1. Free energy diagrams for the electrochemical reduction of CO_2 to CO on flat (Ag(100) and Ag(111)) and edge (Ag(221) and Ag(110)) surfaces. The first two steps include a simultaneous proton/electron transfer, with the final molecular surface configuration at each step depicted on the bottom of the graph. Values of ΔG are reported with an applied potential of −0.11 V vs RHE. Sphere colors: white, H; black, C; red, O; silver, Ag.

that Ag surfaces with steps and edges exhibit significantly lower free energy changes for the first proton-coupled electron transfer in CO_2 reduction in comparison to those for flat surfaces. In particular, $COOH_{ads}$ is more stabilized on Ag(211) by an additional 0.3 eV in comparison to Ag(111). A similar trend is observed for the CO_{ads} step, as Ag(211) exhibits a lower overall free energy change without overbinding. Since both nanoporous and nanoparticle Ag have relatively high densities of stepped sites, these materials should outperform bulk Ag experimentally if the formation of this intermediate is an important step in the mechanism. Note that the proton and electron donation are coupled in the models, as it is still difficult to decouple these steps computationally. In order to further understand the fundamental mechanism, experimental methods must be used.

To better understand the behaviors of nanostructured Ag catalysts and test our hypothesis, we compared the electrochemical CO_2 reduction performances of bulk Ag, Ag nanoparticles, and nanoporous Ag catalysts under various overpotentials. The information regarding the catalyst structural characterizations and corroborating electrochemical surface area measurements can be found in Figures S3−S5 in the Supporting Information. The results from the Tafel analysis are shown in Figure 2a. At low overpotentials, the reaction is mainly kinetically limited, while at higher potentials the slope increases dramatically, indicating that the reaction most likely reaches its mass transport limitations. As expected, this phenomenon is more significant in the cases of nanostructured Ag electrodes, because mass transport in a confined space (nanostructure, curved surface) is much slower than that in an open space (bulk, flat surface). Additional experimental evidence is provided in Figure S6 in the Supporting

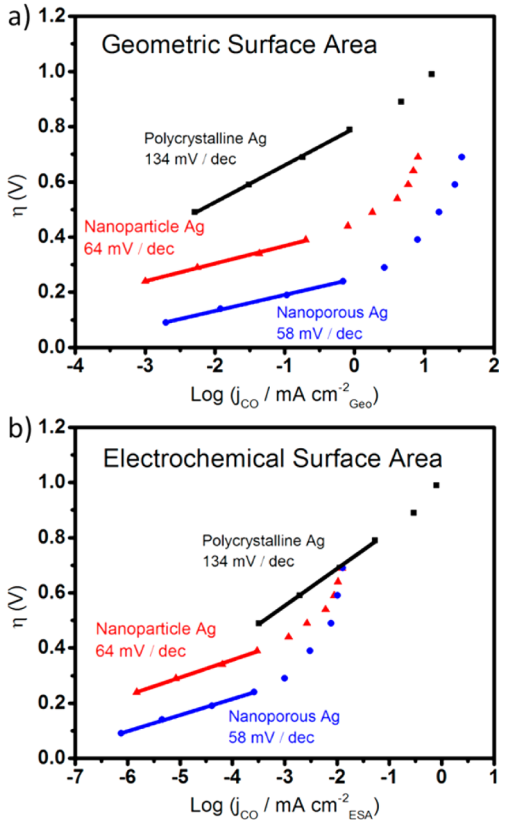

Figure 2. Plot of overpotential (η) vs CO current density (j_{CO}) for bulk Ag and nanostructured Ag catalysts normalized by (a) geometric and (b) electrochemical surface areas.

Information to demonstrate that the rapid increase of slope at high current density is mainly due to mass transport limitations. It can be seen that the nanoporous and nanoparticle Ag catalysts outperform bulk Ag by over 3 and 2 orders of magnitude, respectively, on a geometric basis when 0.5 V of overpotential is applied, which is significantly greater than the increase in surface area measured using electrochemical monolayer oxidation. To further emphasize the intrinsic improvement in catalytic activity, the plots of current normalized to electrochemical surface area are shown in Figure 2b. It can be easily seen that the nanostructured catalysts outperform the bulk Ag even on a per-site basis at low overpotentials where the reaction is kinetically limited. At higher overpotentials of around 0.5 V and greater, mass transport limitations negatively affect the activity of nanostructured catalysts yielding similar activities on a per site basis. These catalysts still greatly outperform bulk Ag on a geometric area basis until much higher overpotentials are reached. The higher per-site activity of nanoporous Ag in comparison to that of nanoparticle Ag is likely due to the higher density of stepped sites.

The DFT modeling results in Figure 1 are in good agreement with our experimental observation of a much higher CO current density on nanostructured surfaces in comaprison to that of bulk Ag, despite the relatively small amount of edges and steps in such large particles. If it is assumed that the additional barrier on top of the free energy difference remains approximately constant for all the Ag surfaces, the expected reaction rate for Ag(211) is roughly 6 orders higher than those of flat surfaces, indicating the important role of nanostructuring.

DOI: 10.1021/acscatal.5b00840
ACS Catal. 2015, 5, 4293−4299

A similar phenomenon was also observed for other nanostructured Ag, Au, and Cu catalysts.[10,23,24]

The overall reaction mechanism of electrochemical reduction of CO_2 to CO on bulk metal catalysts in an aqueous electrolyte has been studied in previous literature. However, the mechanism on nanostructured metallic catalysts has been severely understudied. On bulk Ag, key reaction intermediates have been suggested, starting with an adsorbed CO_2^- radical after a rate-determining initial electron transfer.[15,25] To date, the formation of this radical on the surface of the electrode has been largely understudied. In the course of our computational analysis of CO_2 reduction on Ag surfaces, we have considered an array of possible CO_2 and CO_2^- adsorption configurations and found it highly unlikely that such an intermediate would form on the metallic surface (no stable interaction with Ag is found to exist). Instead, we propose the following mechanism on Ag in aqueous [HCO_3^-] electrolyte:

$$CO_2 + HCO_3^- + e^- + * \rightarrow COOH_{ads} + CO_3^{2-} \quad (A1)$$

$$COOH_{ads} + H_2O + e^- \rightarrow CO_{ads} + H_2O + OH^- \quad (A2)$$

$$CO_{ads} \rightarrow CO + * \quad (A3)$$

Note that * denotes a surface active site. In the first step of the electrocatalytic reduction of CO_2, the transfer of a proton via [HCO_3^-] and an electron to the CO_2 molecule occurs above an available surface site of the metallic electrode, leading to the formation of adsorbed COOH. It is important to note that in electrolytes other than [HCO_3^-] the initial donor may vary. Even in this system, there is the possibility that HCO_3^- reacts reversibly with water, leading to the formation of H_3O^+, which then interacts with CO_2 in the initial proton donation step. This sequence also matches our experimental data, and so we suggest the following alternative to reaction A1 as well, in which the combined proton and electron transfer is preceded by the interaction of HCO_3^- with H_2O:

$$HCO_3^- + H_2O \leftrightarrow H_3O^+ + CO_3^{2-} \quad (A1\text{-}1)$$

$$CO_2 + H_3O^+ + e^- + * \rightarrow COOH_{ads} + H_2O \quad (A1\text{-}2)$$

Though we have performed the DFT studies as presented in Figure 1, decoupling the proton and electron donations remains impossible computationally; therefore, greater insight regarding proton donor species and sequence should be based on experimental work. Subsequent steps include an additional proton and electron transfer, followed by desorption of CO from the surface. Further reduction of CO_2 is typically rare on Ag due to the weak CO adsorption strength.[26−28]

Further insights into the mechanism of CO_2 reduction on Ag can also be ascertained on the basis of a Tafel analysis. On bulk Ag the Tafel slope of 133 mV dec^{-1} normally indicates that the rate-determining step is the initial 1e$^-$ reduction of CO_2.[13] If a combined one-electron/one-proton rate-limiting process is assumed, then the CO partial current can be described as (on the basis of reaction A1)

$$i_{CO} = nFk_{A1}P_{CO_2}[HCO_3^-](1-\theta)\exp\left(\frac{-\beta EF}{RT}\right) \quad (1)$$

where θ is the total surface coverage, E is the applied potential, P_{CO_2} is the partial pressure of CO_2, k_{A1} is a rate constant for reaction A1, β is the symmetry factor and is assumed to be equal to 0.5, F is Faraday's constant, R is the gas constant, and T is the temperature.[29] With an assumption of low surface coverage, the derived value of the Tafel slope ($-\delta E/\delta \log i_{CO}$) is $2.3RT/\beta F$, or 118 mV dec^{-1}. The expected Tafel slope of around 118 mV dec^{-1} is consistent with the slope of the bulk Ag electrode and previous studies suggesting that the one-electron process represented in reaction A1 is rate limiting for CO_2 reduction on bulk Ag surfaces.[13,29]

In sharp contrast, nanostructured Ag shows a clear decrease in the Tafel slope to approximately 60 mV dec^{-1}, indicating a fast initial electron transfer on nanostructured Ag surfaces.[14] We hypothesize that the increased stabilization of this key intermediate reduces the potential needed to overcome this free energy barrier in comparison to bulk Ag.[13] Following this fast combined proton and electron donation step is likely a rate-limiting second proton donation from H_2O, splitting reaction A2 into

$$COOH_{ads} + H_2O \xrightarrow[\text{RDS, nano}]{} COOH_{ads}\cdots H^+ + OH^- \quad (A2\text{-}1)$$

$$COOH_{ads}\cdots H^+ + e^- \rightarrow CO_{ads} + H_2O \quad (A2\text{-}2)$$

On the basis of this hypothesis, our rate expression can be rewritten to be dependent on the surface coverage of the $COOH_{ads}$ intermediate, with the adsorption of $COOH_{ads}$ in fast equilibrium:

$$i_{CO} = nFk_{A2\text{-}1}\theta_{COOH}[H_2O] \quad (2)$$

where θ_{COOH} is the surface coverage of $COOH_{ads}$. If the surface coverage of the CO_2 intermediate is assumed to be very small ($\theta \ll 1$), the expression can be simplified and the new Tafel slope can be determined using eq 3 (see pages S13 and S14 in the Supporting Information):

$$i_{CO} = nFK_{A1}k_{A2\text{-}1}\exp\left(\frac{-EF}{RT}\right)P_{CO_2}\frac{[HCO_3^-][H_2O]}{[CO_3^{2-}]} \quad (3)$$

At this coverage limit, the derived value of the Tafel slope is $2.3RT/F$, or 59 mV dec^{-1}. The analysis shows that the theoretical value of the Tafel slope on the basis of our hypothesized mechanism is consistent with the value observed in the experiments. Therefore, it is likely that nanostructured Ag surfaces are able to stabilize the CO_2 intermediate, leading to different behavior in comparison to bulk Ag catalysts.

In this derivation, we assume that the surface coverage of the CO_2 intermediate is small relative to the total number of active sites on the silver catalyst. It is important to examine other possible rate-determining steps and other scenarios such as moderate and high surface coverage to further justify this claim, and so we present a more complete analysis of the expected Tafel slopes as a function of surface coverage in Table 1 (additional analysis and an expanded derivation can be found in pages S14−S20 in the Supporting Information). This microkinetic analysis follows methods similar to those employed for electrochemical oxygen reduction in previous studies.[30] At the low coverages we expect for nanostructured Ag at low overpotential, only step A2-1 as the rate-determining step produces the expected Tafel slopes of 59 mV dec^{-1}, in agreement with our experimental result. Choosing step A1 instead produces a slope of 118 mV dec^{-1}, which decreases to 59 mV dec^{-1} at intermediate coverage. However, while increasing intermediate coverage should cause an increase in Tafel slope, in the case of step A1 the slope would decrease.

DOI: 10.1021/acscatal.5b00840
ACS Catal. 2015, 5, 4293−4299

Table 1. Expected Coverage Dependences for Each Possible Rate-Determining Step[a]

step	Tafel slope	slope (mV dec^{-1}) low θ	slope (mV dec^{-1}) high θ
A1	$\frac{2.3RT}{F(\beta_{A1} + \theta_{COOH} + \theta_{C-H})}$	118	39
A2-1	$\frac{2.3RT}{F(1 - \theta_{COOH} + \theta_{C-H})}$	59	∞
A2-2	$\frac{2.3RT}{F(\beta_{A2-2} + 1 - \theta_{COOH} - \theta_{C-H})}$	39	118
A2 (combined)	$\frac{2.3RT}{F(\beta_{A2} + 1 - \theta_{COOH})}$	39	118
A3	$\frac{2.3RT}{F(2 - \theta_{COOH} - \theta_{C-H} - 2\theta_{CO})}$	30	∞

[a]Coverage of $COOH_{ads}\cdots H^+$ is written as θ_{C-H}.

Identifying the correct rate-determining step requires more information than the experimental Tafel slope can provide, since it can be easily seen from Table 1 that a Tafel slope of 59 mV dec^{-1} could be obtained from step A2-2, A2, or A3 with moderate coverages. To further verify our claim of step A2-1 as the true rate-determining step, we have examined the CO_2 partial pressure dependence of the Ag catalysts. The effect of CO_2 partial pressure on nanostructured and bulk Ag catalyst activities is shown in Figure 3a–c. It can be seen that for all Ag electrodes the slope of CO current density (i.e., CO production rate) versus CO_2 partial pressure is approximately 0.5. This appears to be in partial agreement with the rate expression shown in eq 6, which shows a dependence on the partial pressure of CO_2. Additionally, this shows that as the partial pressure is increased, the activity of the catalyst also increases, at least in the range of pressures considered here. The deviation from the expected first-order dependence stems from the fact that the pH of the electrolyte changes as parameters such as CO_2 partial pressure are varied, as shown in Tables S1 and S2 in the Supporting Information, which causes a shift in the reversible potential. It should be noted that partial pressure dependence studies have been performed in the case of oxide-derived Au under constant-potential conditions and a slope close to 1 was observed, and we also observe this behavior on our nanostructured Ag materials (Figure S7 in the Supporting Information).[13] In addition, other reports have analyzed this dependence but the details were not well reported.[31] However, our data suggest that it is more appropriate to study the dependence of the rate equation on CO_2 partial pressure with constant overpotential because of the shift of reversible potential resulting from the change of concentration. These considerations can be accounted for by applying the Nernst equation, as

$$E = E^{rev} - \eta \tag{4}$$

$$E^{rev} = E^{\circ} - \frac{2.3RT}{2F}\log\left(\frac{[OH^-][CO_3^{2-}]P_{CO}}{P_{CO_2}[HCO_3^-]}\right) \tag{5}$$

on the basis of the overall reaction

$$CO_2 + HCO_3^- + H_2O + 2e^- \leftrightarrow CO + OH^- + CO_3^{2-} + H_2O \tag{6}$$

It can be therefore be seen from this analysis that an expected slope of 0.5 in the partial pressure dependence study is expected, indicating an actual first-order overall dependence (a more complete derivation is provided in pages S13–S14 in the Supporting Information).

It should be noted that for bulk Ag there are multiple conditions which result in an observed Tafel slope of

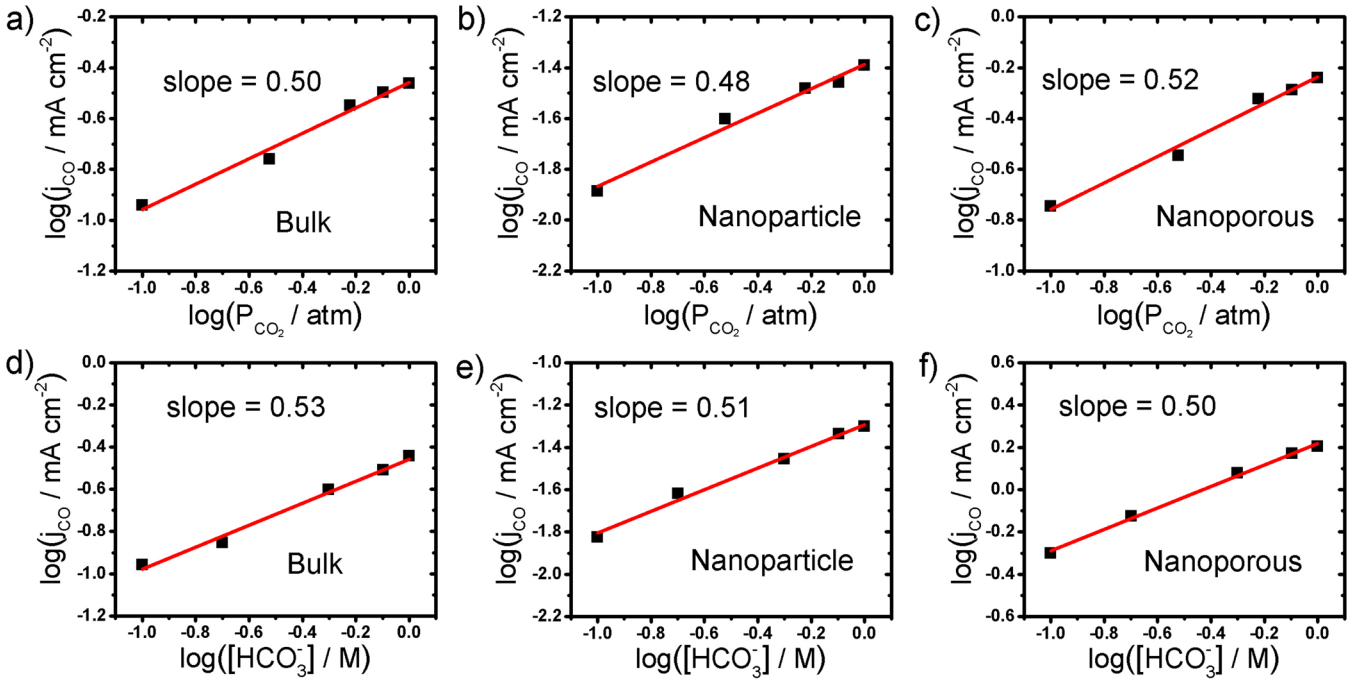

Figure 3. CO_2 partial pressure dependence studies performed at constant overpotentials for (a) bulk Ag, (b) nanoparticle Ag, and (c) nanoporous Ag and bicarbonate concentration dependence studies performed at constant overpotentials for (d) bulk Ag, (e) nanoparticle Ag, and (f) nanoporous Ag.

DOI: 10.1021/acscatal.5b00840
ACS Catal. 2015, 5, 4293–4299

approximately 120 in addition to the proposed rate-limiting process. It is possible that coverage effects may be significant, unlike in the case of nanostructured Ag. The higher coverage may stem from a lower availability of active sites or the overbinding of adsorbed reaction intermediates on a highly negatively charged electrode surface. As long as coverage does not change significantly in the Tafel region, a linear Tafel slope will still be observed. This is in contrast to the previously made assumption indicating a rate-limiting step on bulk Ag potentially different from electron donation.[11,13,23]

Furthermore, since bulk Ag has a low electrochemical surface area of ∼1 cm^2, the lowest CO current that can be measured accurately is approximately 0.1 μA (i.e., $j_{CO} = 1 \times 10^{-4}$ mA cm^{-2} ESA). Comparatively, CO currents below 1×10^{-6} mA cm^{-2} ESA can be accessed on nanostructured Ag (Figure 2b). While a Tafel slope of 133 mV dec^{-1} could be estimated on bulk (based on data obtained at η = 0.5−0.8 V), the slope may not be truly kinetically limited due to the use of larger overpotentials needed to measure significant amounts of product. It is very likely that other factors such as surface coverage on the bulk Ag surface strongly influence the slope under testing conditions (i.e., high overpotentials). For example, the Tafel slope on bulk Ag would be approximately 59 mV dec^{-1} when a coverage of 0 can be achieved, reaching 118 mV dec^{-1} when θ = 0.5 and increasing indefinitely as the coverage approaches unity.

The expected nonlinearity may be difficult to see experimentally due to only small changes in coverage in the Tafel region on bulk Ag. Moreover, the reaction order with respect to P_{CO_2} now depends on θ. These results yield a strong possibility that the mechanism on bulk Ag is identical with that of nanostructured Ag with the same rate-determining step but instead operates in a different coverage regime. Further experiments may be required to obtain a comprehensive understanding of the reaction mechanism for bulk Ag. In addition to looking at factors such as coverage, other effects such as surface contamination from the electrolyte should be considered, as they are more likely to affect bulk metallic catalysts in comparison to nanostructured materials. It should be noted that in this study high-purity electrolytes and preventative measures such as pre-electrolysis were used to minimize this effect.

To further explain our hypothesized reaction mechanism on nanostructured Ag catalysts, we have also studied the bicarbonate concentration dependence. For all Ag catalysts, a slope of approximately 0.5 was observed, as shown in Figure 3d−f, highlighting that the bicarbonate ions are directly involved in the CO_2 to CO catalytic conversion. This indicates a true first-order dependence on bicarbonate concentration for nanostructured Ag and bulk Ag, and as described previously (see pages S13−S14 in the Supporting Information), the observed fractional order stems from a shift in the reversible potential. The similarity between bulk and nanostructured Ag further highlights a potential similar mechanism, albeit while operating in different coverage regimes. It can therefore be seen that a slope of 0.5 in the bicarbonate concentrate study is indeed expected if the initial proton donation is from bicarbonate while the rate-determining step is the proton donation from water. This theoretical value agrees well with our experimental observations. It is likely that, once adsorbed, $COOH_{ads}$ is unable to accept a proton given from $[HCO_3^-]$ due to the low concentration of these negatively charged ions near the negatively charged Ag surface. Therefore, the source of proton donation in the second step is likely from water instead. Furthermore, assuming that $[HCO_3^-]$ is both the first and also the second proton donor produces an expected dependence that is inconsistent with the data (Table S4 in the Supporting Information). The influence of surface coverage of other intermediates on Tafel slope and reactant dependences has also been examined and shown in pages S12−S19 in the Supporting Information. The analysis further confirmed the proposed rate-determining step in the overall mechanism on nanostructure Ag.

Given that both P_{CO_2} and $[HCO_3^-]$ dependences observed for nanostructured Ag match the expected values for step A2-1 as the rate-determining step if θ_{COOH} is low, we maintain that the current density is low enough on nanostructured Ag to observe the true Tafel regime. Both A2-2 and A2 as the rate-determining steps would exhibit lower Tafel slopes in the case of low θ_{COOH}. Furthermore, while A3 as the rate-determining step provides the possibility for θ_{CO} dependence, it has been observed that CO does not strongly adsorb on Ag, with gaseous CO greatly favored over adsorbed CO and an adsorption energy of CO more than 0.3 eV weaker than that for Au.[32] Given previous results showing that θ_{CO} is low on Au operating at low overpotentials, we expect that θ_{CO} should be very low in Ag and step is also excluded as the rate-determining step.[33] Therefore, we propose that A2-1, the protonation of adsorbed *COOH* following the first proton-coupled electron transfer, is the rate-determining step for CO_2 reduction on nanostructured Ag surfaces.

The near-identical Tafel slopes and bicarbonate dependence for both nanoporous and nanoparticle Ag catalysts indicate a similar reaction mechanism for CO_2 reduction. Our results suggest that the dissolved CO_2 molecule accepts one electron and one proton from the electrode and HCO_3^- to form adsorbed COOH at the nanostructured Ag surface. Because the low-coordinated surface Ag sites are able to stabilize the formed COOH through reducing the activation energy barrier of the first electron transfer, the specific activity is increased. Following the second proton donation step, there is a relatively fast second electron transfer and ultimately desorption of CO from the catalyst surface. When a similar derivation is performed for the bulk Ag rate expression, it can be seen that the 0.5 bicarbonate dependence shown in Figure 3d is also consistent with the described mechanism where step A1 is rate limiting as well.

The new mechanism of CO_2 to CO conversion on the surface of nanostructured Ag catalysts clearly demonstrates the important role of nanostructuring, which was also seen in other recent discoveries involving nanoarchitectured Ag, Au, and Cu catalysts.[10,23,24] On the basis of the study presented in this article, it is believed that the metal atoms positioned on a highly nanostructured surface play an important role in facilitating the electrocatalytic conversion of CO_2 to reduced species, resulting in distinct behaviors of nanostructured catalysts in comparison to bulk catalysts, as shown in the cases of nanoporous and nanoparticle Ag.

CONCLUSION

In summary, insights into the mechanism of CO_2 reduction on nanostructured Ag catalysts were obtained through a series of experimental and computational modeling studies. Investigation into the activity of nanostructured Ag catalysts further

DOI: 10.1021/acscatal.5b00840
ACS Catal. 2015, 5, 4293−4299

highlighted the unique ability of low-coordinated surface Ag atoms (active sites) to improve CO production rates and selectivity. The second proton donation step was found to be the rate-determining step for CO_2 to CO conversion on nanostructured Ag. A new CO_2 reduction reaction mechanism that matches observed kinetic, CO_2 partial pressure, and $[HCO_3^-]$ dependence properties was proposed for Ag catalysts. Further experiments may be required to obtain a comprehensive understanding of the reaction mechanism of Ag-based catalysts for CO_2 reduction, particularly for low-surface-area bulk materials.

■ ASSOCIATED CONTENT

Supporting Information

The Supporting Information is available free of charge on the ACS Publications website at DOI: 10.1021/acscatal.5b00840.

High-angle PXRD patterns of as-made Ag catalysts, SEM images of Ag electrodes, electrochemically active surface areas of Ag catalysts, gas chromatography, NMR, details for computational methods, and summary of alternate reaction schemes (PDF)

■ AUTHOR INFORMATION

Corresponding Author

*E-mail for F.J.: jiao@udel.edu.

Author Contributions

§These authors contributed equally to this work.

Notes

The authors declare no competing financial interest.

■ ACKNOWLEDGMENTS

Acknowledgment is made to the National Science Foundation Faculty Early Career Development program (Award No. CBET-1350911). The computational work in this study was financially supported by a University of Delaware Research Foundation Strategic Initiatives (UDRF-SI) grant. The authors thank Dr. Yushan Yan for providing anion exchange membranes.

■ REFERENCES

(1) Benson, E. E.; Kubiak, C. P.; Sathrum, A. J.; Smieja, J. M. *Chem. Soc. Rev.* **2009**, *38*, 89−99.

(2) Rakowski Dubois, M.; Dubois, D. L. *Acc. Chem. Res.* **2009**, *42*, 1974−1982.

(3) Kumar, B.; Llorente, M.; Froehlich, J.; Dang, T.; Sathrum, A.; Kubiak, C. P. *Annu. Rev. Phys. Chem.* **2012**, *63*, 541−569.

(4) Costentin, C.; Robert, M.; Savéant, J.-M. *Chem. Soc. Rev.* **2013**, *42*, 2423−2436.

(5) Kondratenko, E. V.; Mul, G.; Baltrusaitis, J.; Larrazabal, G. O.; Perez-Ramirez, J. *Energy Environ. Sci.* **2013**, *6*, 3112−3135.

(6) Grice, K. A.; Kubiak, C. P. In *CO_2 Chemistry*; Aresta, M., van Eldik, R., Eds.; Academic Press: New York, 2014; Advances in Inorganic Chemistry *66*, pp 163−188.

(7) Lu, Q.; Rosen, J.; Jiao, F. *ChemCatChem* **2015**, *7*, 38−47.

(8) Qiao, J.; Liu, Y.; Hong, F.; Zhang, J. *Chem. Soc. Rev.* **2014**, *43*, 631−675.

(9) Zhang, S.; Kang, P.; Meyer, T. J. *J. Am. Chem. Soc.* **2014**, *136*, 1734−1737.

(10) Zhu, W.; Michalsky, R.; Metin, Ö.; Lv, H.; Guo, S.; Wright, C. J.; Sun, X.; Peterson, A. A.; Sun, S. *J. Am. Chem. Soc.* **2013**, *135*, 16833−16836.

(11) Hori, Y. In *Modern Aspects of Electrochemistry*; Vayenas, C. G., White, R. E., Gamboa-Aldeco, M. E., Eds.; Springer: Berlin, 2008; Vol. *42*, pp 89189.

(12) Kuhl, K. P.; Cave, E. R.; Abram, D. N.; Jaramillo, T. F. *Energy Environ. Sci.* **2012**, *5*, 7050−7059.

(13) Chen, Y.; Li, C. W.; Kanan, M. W. *J. Am. Chem. Soc.* **2012**, *134*, 19969−19972.

(14) Lu, Q.; Rosen, J.; Zhou, Y.; Hutchings, G. S.; Kimmel, Y. C.; Chen, J. G.; Jiao, F. *Nat. Commun.* **2014**, *5*, 3242.

(15) Hatsukade, T.; Kuhl, K. P.; Cave, E. R.; Abram, D. N.; Jaramillo, T. F. *Phys. Chem. Chem. Phys.* **2014**, *16*, 13814−13819.

(16) Rosen, B. A.; Salehi-Khojin, A.; Thorson, M. R.; Zhu, W.; Whipple, D. T.; Kenis, P. J. A.; Masel, R. I. *Science* **2011**, *334*, 643−644.

(17) Peterson, A. A.; Nørskov, J. K. *J. Phys. Chem. Lett.* **2012**, *3*, 251−258.

(18) Hammer, B.; Hansen, L.; Nørskov, J. *Phys. Rev. B: Condens. Matter Mater. Phys.* **1999**, *59*, 7413−7421.

(19) Kresse, G.; Furthmüller, J. *Comput. Mater. Sci.* **1996**, *6*, 15−50.

(20) Kresse, G. *Phys. Rev. B: Condens. Matter Mater. Phys.* **1996**, *54*, 11169−11186.

(21) Nørskov, J. K.; Rossmeisl, J.; Logadottir, A.; Lindqvist, L.; Kitchin, J. R.; Bligaard, T.; Jónsson, H. *J. Phys. Chem. B* **2004**, *108*, 17886−17892.

(22) Peterson, A. A.; Abild-Pedersen, F.; Studt, F.; Rossmeisl, J.; Norskov, J. K. *Energy Environ. Sci.* **2010**, *3*, 1311−1315.

(23) Li, C. W.; Kanan, M. W. *J. Am. Chem. Soc.* **2012**, *134*, 7231−7234.

(24) Salehi-Khojin, A.; Jhong, H.-R. M.; Rosen, B. A.; Zhu, W.; Ma, S.; Kenis, P. J. A.; Masel, R. I. *J. Phys. Chem. C* **2012**, *117*, 1627−1632.

(25) Hori, Y.; Wakebe, H.; Tsukamoto, T.; Koga, O. *Electrochim. Acta* **1994**, *39*, 1833−1839.

(26) Gattrell, M.; Gupta, N.; Co, A. *J. Electroanal. Chem.* **2006**, *594*, 1−19.

(27) Hansen, H. A.; Varley, J. B.; Peterson, A. A.; Nørskov, J. K. *J. Phys. Chem. Lett.* **2013**, *4*, 388−392.

(28) Hoshi, N.; Kato, M.; Hori, Y. *J. Electroanal. Chem.* **1997**, *440*, 283−286.

(29) Gileadi, E. *Physical Electrochemistry: Fundamentals, Techniques, and Applications*, 1st ed.; Wiley-VCH: Weinheim, Germany, 2011.

(30) Holewinski, A.; Linic, S. *J. Electrochem. Soc.* **2012**, *159*, H864−H870.

(31) Manthiram, K.; Beberwyck, B. J.; Alivisatos, A. P. *J. Am. Chem. Soc.* **2014**, *136*, 13319−13325.

(32) Kuhl, K. P.; Hatsukade, T.; Cave, E. R.; Abram, D. N.; Kibsgaard, J.; Jaramillo, T. F. *J. Am. Chem. Soc.* **2014**, *136*, 14107−14113.

(33) Akhade, S. A.; Luo, W.; Nie, X.; Bernstein, N. J.; Asthagiri, A.; Janik, M. J. *Phys. Chem. Chem. Phys.* **2014**, *16*, 20429−20435.

DOI: 10.1021/acscatal.5b00840
ACS Catal. 2015, 5, 4293−4299